第 50 卷第 11 期 中国科学技术大学学报 Vol. 50, No. 11
2020 年 11 月 JOURNAL OF UNIVERSITY OF SCIENCE AND TECHNOLOGY OF CHINA Nov. 2020
Received：2020-09-23；Revised：2020-11-19 doi:10.3969/j.issn.0253-2778.2020.11.002

Recent achievements in solution processed antimony selenosulfide solar cells

JIANG Chenhui, TANG Rongfeng, ZHU Changfei*, CHEN Tao*
Hefei National Laboratory for Physical Sciences at the Microscale, CAS Key Laboratory of Materials for Energy Conversion, Department of Materials Science and Engineering, University of Science and Technology of China, Hefei 230026, China
*Corresponding author：cfzhu@ustc.edu.cn；tchenmse@ustc.edu.cn

Abstract：Antimony selenosulfide, $Sb_2(S,Se)_3$, displays superior optoelectronic properties such as strong absorption coefficient and easily tunable bandgap in the range of 1.1～1.7 eV. In terms of practical photovoltaic applications, this semiconductor material is relatively non-toxic, low cost, earth abundant, and stable against moisture and air. Recent investigations have witnessed the rapid development with the power conversion efficiency overcoming the 10% bottleneck in $Sb_2(S,Se)_3$ solar cells, demonstrating great potential for further investigations. In this perspective, the structural, crystal and optical properties of $Sb_2(S,Se)_3$ are introduced first, and then notable developments are highlighted, primarily in the past three years, in $Sb_2(S,Se)_3$ solar cells with film deposition by solution based methods. Finally, some possible strategies are proposed with regard to efficiency improvement.

Keywords：solar cell; antimony selenosulfide; $Sb_2(S,Se)_3$; solution process; hydrothermal deposition
CLC number：TM914.4 **Document code**：A

1 Introduction

Antimony selenosulfide, $Sb_2(S,Se)_3$, has emerged as a promising alternative absorber material due to its tunable bandgap ranging from 1.1 to 1.7 eV, high absorption coefficients at visible range ($>10^5$ cm^{-1}), and large dielectric constant (>15)[1-3]. Moreover, $Sb_2(S,Se)_3$ is low-cost, earth-abundant, low-toxicity, and air-stable, which makes it an excellent candidate for solar cell applications[4-6]. The low melting point as well as high vapor pressure for $Sb_2(S,Se)_3$ allows the low-temperature fabrication of high-quality films[7].

$Sb_2(S,Se)_3$ crystallizes into an orthorhombic structure, which belongs to the P_{nma}(#62) space group. In particular, $Sb_2(S,Se)_3$ structure consists of $[Sb_4S(Se)_6]_n$ chains (ribbons) along the [001] direction, while the ribbons are weakly bonded by van der Waals forces along the *a* and *b* directions. This ribbon structure presents the film with significantly reduced number of dangling bonds (Fig. 1(a),(b)). Furthermore, this one-dimensional (1D) crystal structure exhibits anisotropy in electrical conductivity, edge absorption and carrier transport along different orientations. Recent studies also revealed a unique characteristic of the 1D structure: if the orientation of the $[Sb_4S(Se)_6]_n$ atomic chains is well controlled and perpendicular to the p-n junction interface in the solar cells, the grain boundaries in these 1D semiconductors can be intrinsically benign since they do not produce interface states in the bandgap and thus cause no non-radiative recombination, leading to highly efficient carrier transport[8,9].

$Sb_2(S,Se)_3$ is isostructural with Sb_2S_3 and Sb_2Se_3, the increase in S/Se atomic ratio leads to a gradual upshift of X-ray diffraction peaks positions since the diameters of Se and S atoms are 1.17 Å and 1.04 Å, respectively. The manipulation on the atomic ratio renders the onset of UV-vis absorption tunable from 720 nm to 1100 nm, corresponding to the bandgap variation in the range of 1.72 eV to 1.13 eV(Fig. 1(d)～(f)). According to the Shockley-Queisser limit, the band gaps of $Sb_2(S,Se)_3$ fall into the optimal values, and the theoretical maximum solar conversion efficiency of single-junction $Sb_2(S,Se)_3$ solar cell can thus reach around 33.7% (Fig. 1(c)).

In general, preparation process of $Sb_2(S,Se)_3$ film is critical for obtaining a high power conversion efficiency (PCE) of $Sb_2(S,Se)_3$ solar cells, since it influences the morphological, electrical and defect properties of $Sb_2(S,Se)_3$ film. The conventional film preparation methods such as the chemical bath deposition, spin-coating method, vapor deposition, as well as hydrothermal deposition method have been

Citation：JIANG Chenhui, TANG Rongfeng, ZHU Changfei, et al. Recent achievements in solution processed antimony selenosulfide solar cells. J. Univ. Sci. Tech. China, 2020, 50(11): 1383-1393.

adopted in the fabrication of $Sb_2(S,Se)_3$ films. Here we focus particularly on the solution-based approaches, analyzing each method by comparison. These device configurations and photovoltaic parameters are summarized in Tab. 1. We wish to inspire new materials processing approaches for high-quality absorber films. Moreover, we will also provide some suggestions for achieving efficiency advance in terms of device architecture, defect passivation and interfacial transport materials.

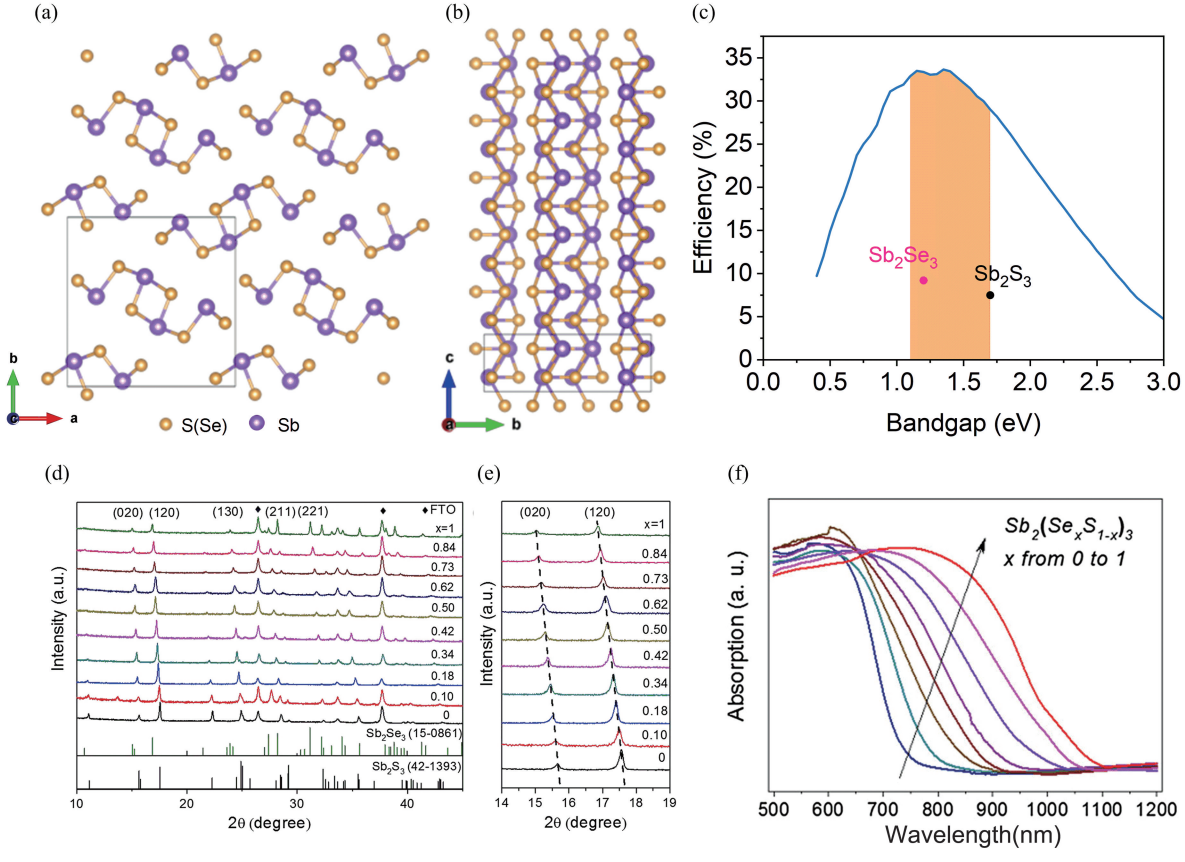

Fig. 1 (a, b) Crystal structure of $Sb_2(S,Se)_3$ along (001) and (100) crystal planes, (c) Theoretical Shockley-Queisser efficiency limit of Sb_2S_3 and Sb_2Se_3 absorber materials. (d, e) XRD patterns and (f) UV-vis absorption spectra of $Sb_2(Se_xS_{1-x})_3$ film. Reproduced permission from Ref.[10]. Copyright 2018, Wiley-VCH.

Tab. 1 Summary of $Sb_2(S,Se)_3$ solar cells configuration, fabrication method, and corresponding photovoltaic parameters.

Method	Cell configuration	V_{OC} (V)	J_{SC} (mA · cm^{-2})	FF(%)	PCE(%)	Ref.
CBD	FTO/c-TiO_2/m-TiO_2/Sb_2S_3/PCPDTBT/Au	0.711	16.1	65.0	7.5	[11]
	FTO/CdS/$Sb_2S_{1.2}Se_{1.8}$/PbSe/C-Ag	0.454	12.5	44	2.5	[12]
	FTO/c-TiO_2/m-TiO_2/$Sb_2(S,Se)_3$/P3HT/Au	0.4748	24.9	55.6	6.6	[13]
	FTO/TiO_2/$Sb_2(S,Se)_3$/Spiro/Au	0.56	19.48	52.34	5.71	[14]
	FTO/CdS/$Sb_2(S,Se)_3$/C-Ag	0.645	10.08	40.6	2.64	[15]
Spin coating	FTO/TiO_2/$Sb_{1.9}S_{2.2}Se_{0.9}$/Spiro/Au	0.52	21.1	52.4	5.8	[16]
	FTO/TiO_2/In:CdS/$Sb_{1.99}S_{2.11}Se_{0.91}$/Spiro/Au	0.59	18.14	62.39	6.63	[17]
	FTO/TiO_2/$Sb_2S_{1.02}Se_{2.21}$/Spiro/Au	0.491	25.4	59.5	7.42	[18]
Hydrothermal	FTO/TiO_2/CdS/$Sb_2(S,Se)_3$/Spiro/Au	0.792	12.03	60.9	5.73	[19]
	FTO/CdS/$Sb_2(S,Se)_3$/Spiro/Au	0.732	14.6	60.8	6.14	[20]
	FTO/CdS/$Sb_2(S,Se)_3$/Spiro/Au	0.655	24.1	63.5	10.0	[21]
	FTO/CdS/$Sb_2(S,Se)_3$/Spiro/Au	0.664	23.8	66.3	10.5	[22]
	FTO/CdS/$Sb_2S_{2.5}Se_{0.38}$/$CsPbBr_3$ QDs/Au	0.62	21.50	58.55	7.82	[23]

2 Solution processed $Sb_2(S,Se)_3$ film for solar cell applications

In general, there are two approaches for the preparation of $Sb_2(S,Se)_3$ films in the solution process. One is the reactive deposition approach, as shown in Fig. 2(a), where the reactive ions or targeting materials are deposited onto the substrate to form multi-crystalline film. This method is usually followed by post-annealing to enhance crystallinity. The typical methods are chemical bath deposition (CBD) and hydrothermal deposition. The other approach is the spin-coating method, where the bulk materials are firstly dissolved with a suitable solvent (Fig. 2(b)). Upon spin coating, a precursor film is formed. The film was annealed at moderate temperature to solidify the film and then annealed at high temperature to enhance the crystallinity. These methods have generated high-quality $Sb_2(S,Se)_3$ films with distinct morphological, electrical and photovoltaic properties. Here we analyze the methods according to the application in the synthesis of $Sb_2(S,Se)_3$ film for solar cell.

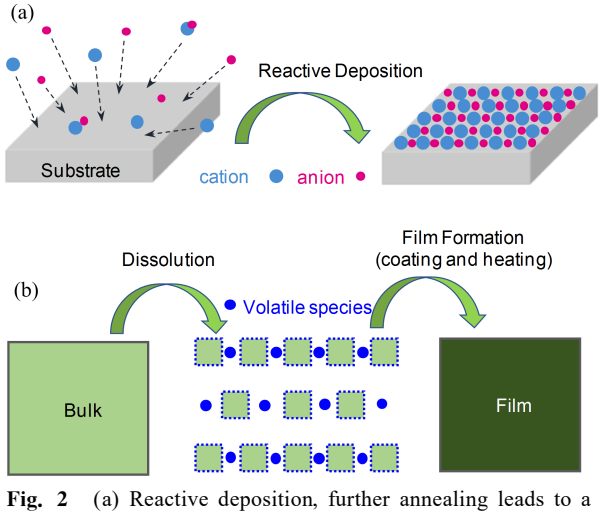

Fig. 2 (a) Reactive deposition, further annealing leads to a polycrystalline film, and (b) spin coating and annealing method.

2.1 Chemical bath deposition and post-treatment

Chemical bath deposition (CBD) is a method to deposit stable, uniform, and solid thin films by a relatively simple solution-based process. This technique has been extensively used to deposit buffer layers such as CdS, In_2S_3 and Zn(O,S) in CdTe and $CuInGaSe_2$ thin film solar cells[24,25]. One of the keys to the CBD process is to use appropriate precursor compounds in the chemical bath. In 2013, Nair group reported a single-step CBD method to deposit $Sb_2S_{1.2}Se_{1.8}$ alloy film on CdS substate by using potassium-antimony tartrate, thioacetamide and selenosulfate as Sb, S, and Se sources[12]. With PbSe film as hole transport material (HTM), the device based on FTO/CdS/$Sb_2S_{1.2}Se_{1.8}$/PbSe/C-Ag delivers PCE of 2.5%. Due to the high charge carrier transport resistance with thick PbSe film and colloidal graphite paint, this cell efficiency is relatively inferior. One year later, Seok and coworkers demonstrated $Sb_2(S,Se)_3$-sensitized solar cells by interreaction and interdiffusion between Sb_2Se_3 and Sb_2S_3[13]. As illustrated in Fig. 3(a), Sb_2S_3 was pre-deposited through the CBD process, followed by spin coating of a single source precursor and thermal decomposition[26,27]. At an elevated temperature, the reaction generates S(Se) gradient $Sb_2(S,Se)_3$ sensitizer. The utilization of poly(3-hexylthiophene) (P3HT) as HTM with optimized compositional gradient leads to the device efficiency reaching 6.6% with a broad IPCE covering the near-IR region up to 1050 nm, which outperforms both Sb_2S_3- and Sb_2Se_3-based cells (Fig. 3(b), (c)). The authors proposed that this synthesis was able to form favorable cascaded band alignment in which the internal electric field facilitates the carrier separation and transport (Fig. 3(d), (e)). It is worthy of noting that for the pure Sb_2S_3 sensitized solar cell, when a post-treatment by thioacetamide (TA) was carried out to heal the defect, the device efficiency reached of 7.5%[11].

This reaction and interdiffusion approach is also applicable in the planar heterojunction device architectures. Zhang et al. synthesized Sb_2S_3 firstly on the surface of compact TiO_2 substrate by CBD (Fig. 4(a)). Afterwards, the pre-dissolved selenium solution was spin-coated onto the surface of Sb_2S_3. Upon annealing at a high temperature, the reaction between Sb_2S_3 and selenium forms $Sb_2(S,Se)_3$. Because of the solid-state reaction, controlling the annealing temperature is able to manipulate the diffusion of reactants that finally generates vertically graded selenium distribution. The planar heterojunction solar cell based on this film delivered an efficiency of 5.71%[14]. Due to the cascaded band alignment of $Sb_2(S,Se)_3$ in the solar cell (Fig. 4(c)), the solar cell can maintain a V_{OC} comparable to the Sb_2S_3-based device while the J_{SC} is two times higher than both of the devices based on Sb_2S_3 and Sb_2Se_3 (Fig. 4(b)). In addition, this band alignment renders the electron injection from $Sb_2(S,Se)_3$ to TiO_2 and hole transport from the valence band of $Sb_2(S,Se)_3$ to the HTM being more energetically favorable.

In addition, solid-gas reaction is another feasible strategy to obtain $Sb_2(S,Se)_3$ film. Wang et al. prepared the graded bandgap $Sb_2(S,Se)_3$ thin film through the post-selenization treatment of CBD-deposited Sb_2S_3 film using Se vapor at a high temperature[15]. Capping with carbon electrode as HTM on $Sb_2(S,Se)_3$, the all-inorganic device delivered a 2.64% PCE. It seems difficult for the carbon paste to form good contact with the absorber film, which increases the charge transport

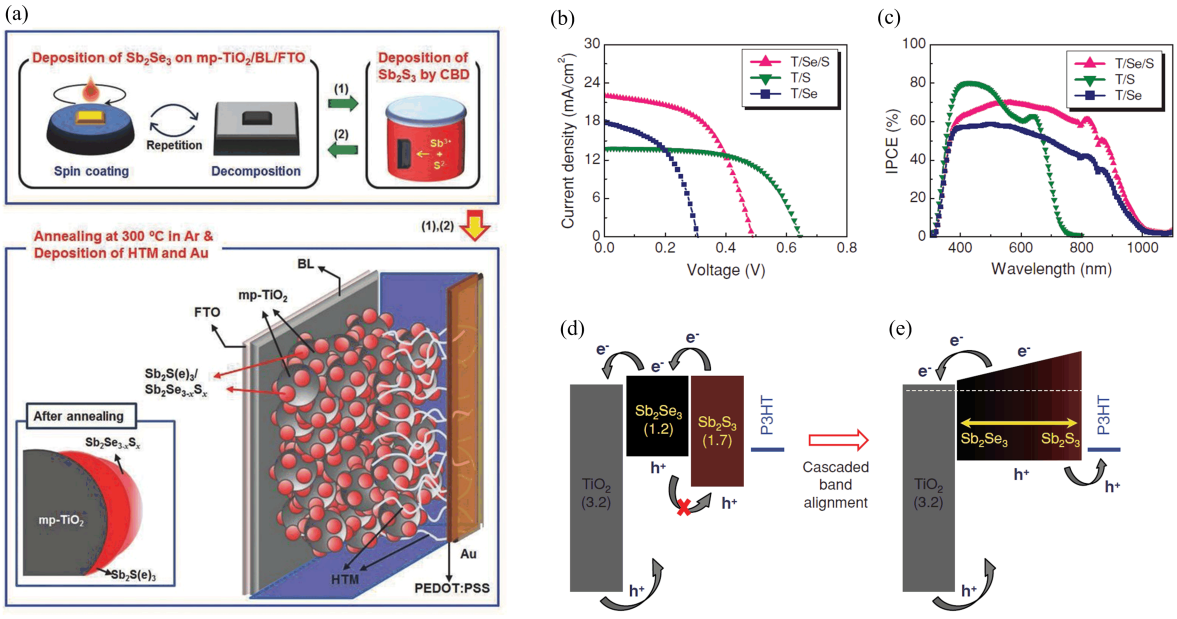

Fig. 3 (a) Schematic illustration of the fabrication process of the inorganic-organic heterojunction solar cells based on $Sb_2(S,Se)_3$ graded-composition sensitizers. (b) *J*-*V* curves and (c) IPCE spectra of the optimized graded $Sb_2(S,Se)_3$-based (T/Se/S), pristine Sb_2S_3-based (T/S), and pristine Sb_2Se_3-based (T/Se) solar cells. (d) Relative energy band diagram of TiO_2, Sb_2Se_3, Sb_2S_3, and P3HT. (e) Proposed cascaded-band alignment on the mp-TiO_2/Sb_2Se_3/Sb_2S_3/P3HT structure. Reproduced with permission from Ref.[13]. Copyright 2014, Wiley-VCH.

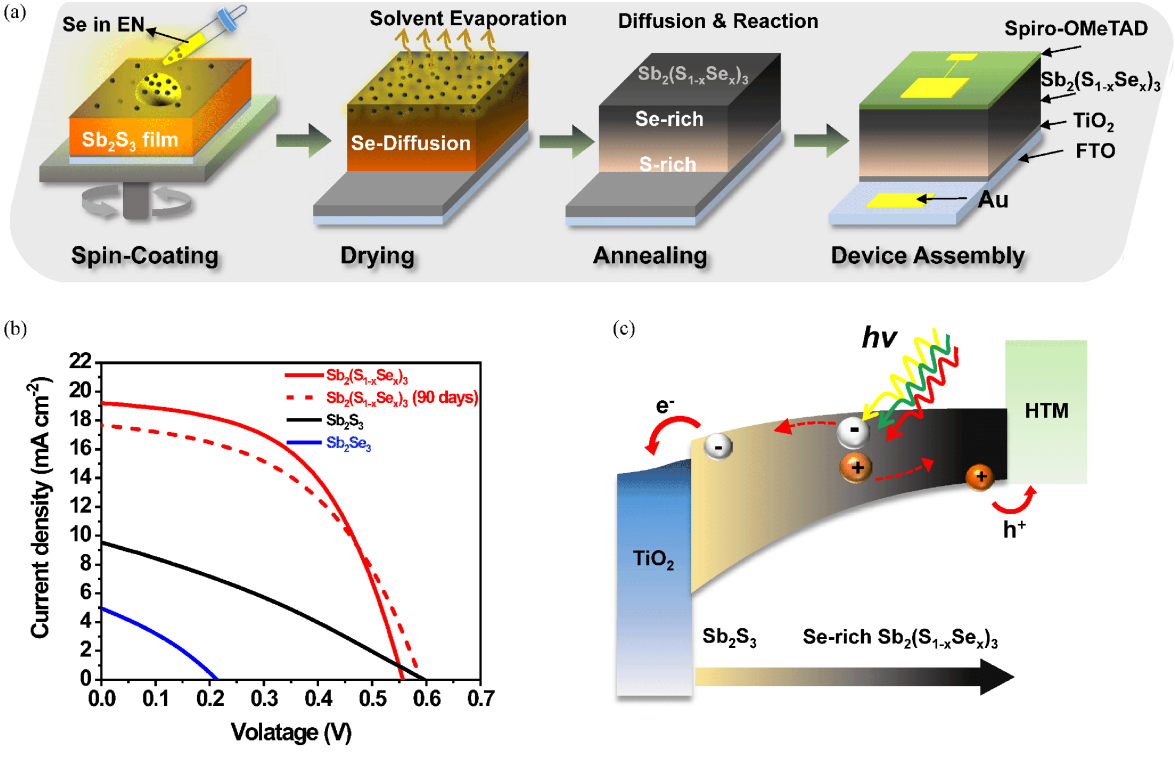

Fig. 4 (a) Schematic illustration of the fabrication of selenium-graded $Sb_2(S,Se)_3$. (b) *J*-*V* curves of the devices based on Sb_2S_3, $Sb_2(S,Se)_3$ and Sb_2Se_3, and $Sb_2(S,Se)_3$-based device storing for 90 d. (c) Diagram of proposed energy band alignment of $Sb_2(S,Se)_3$ solar cells. Reproduced with permission from Ref.[14]. Copyright 2017, Wiley-VCH.

resistance and generates low efficiency when compared with organic HTM based devices.

These results have demonstrated that effective selenization treatment on CBD-processing Sb_2S_3 film

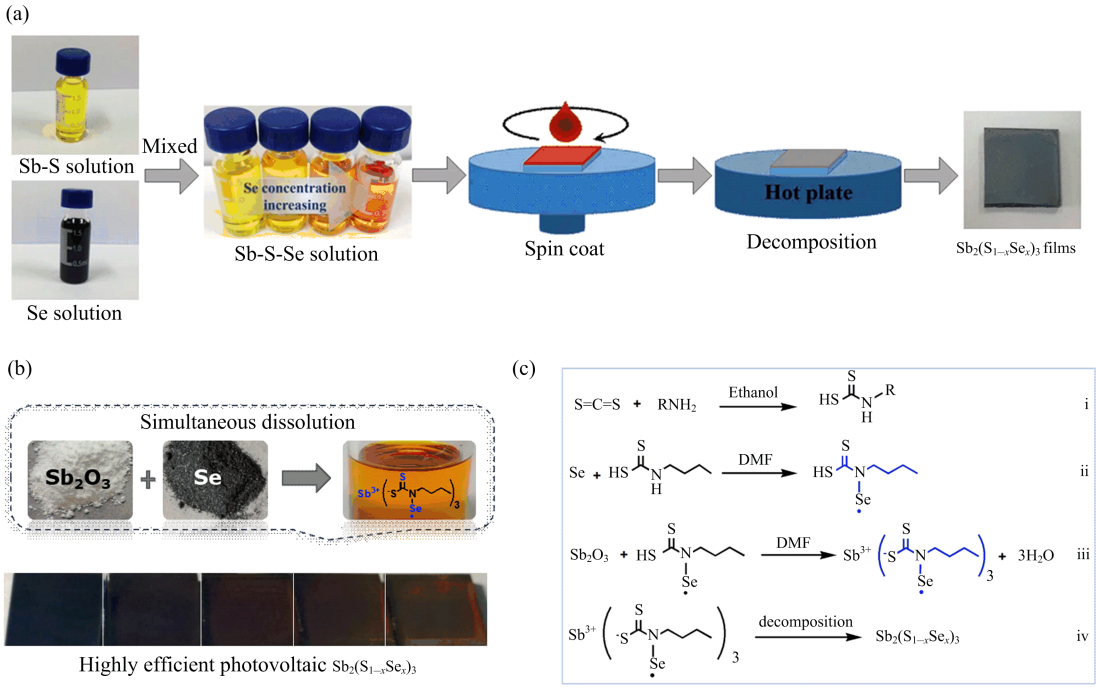

Fig. 5 (a) Schematic illustration of the preparation of $Sb_2(S,Se)_3$ films. Reproduced with permission from Ref.[29]. Copyright 2015, Nature Publishing Group. (b) Simultaneous dissolution of selenium and Sb_2O_3 powder for direct synthesis of photovoltaic $Sb_2S_{3-x}Se_x$ films. (c) Proposed reaction pathways toward the synthesis of $Sb_2(S,Se)_3$. Reproduced with permission from Ref.[16]. Copyright 2018, Elsevier Ltd.

could transfer the film to Se/S composition gradient $Sb_2(S,Se)_3$ for efficient $Sb_2(S,Se)_3$ solar cells. This approach is facile and cost-effective. However, the CBD approach inevitably generates oxide/hydroxide impurity phases[11,28], and further improvements in device performance can be expected by delicately optimizing the fabrication technique.

2.2 Spin-coating method

In the spin-coating process, the molecular precursor solution containing required elements is firstly spin-coated onto the substrate. It is usually followed by low-temperature annealing to evaporate the solvent out and solidify the film and a high-temperature annealing for reaction and crystallization. A typical spin-coating process is shown in Fig. 5(a), where the $Sb_2(S,Se)_3$ thin films were deposited via spin-coating Sb-S-Se precursor solutions by dissolving Sb, S, and Se powders into hydrazine onto TiO_2 substrates, followed by drying on a preheated hot plate at 100 °C, and subsequently annealing at 300 °C[29].

The thiol-amine mixture solvent exhibits strong capability in the dissolution of metal oxide, metal sulfide, element selenium or tellurium or their mixture for the preparation of metal chalcogenide. Brutchey and co-workers prepared $Sb_2(S,Se)_3$ alloys by using Sb_2O_3 and selenium in binary alkanethiol-1,2-ethylenediamine solvent mixtures[30]. Wu et al. demonstrated a method towards simultaneous dissolution of Se and Sb_2O_3 powers in carbon disulfide (CS_2), n-butylamine (nBA) and N,N-dimethylformamide (DMF) mixed solution for direct deposition of alloyed $Sb_2(S,Se)_3$ solar cells via a one-step spin-coating process (Fig. 5(b))[16]. It was found that the formation of selenium-nitrogen free radical in sulfur-containing complex is responsible for the dissolution of selenium powder (Fig. 5(c)). By tuning the atomic ratios between sulfur and selenium in the molecular precursor solution, a series of $Sb_2(S,Se)_3$ films with different Se/S atomic ratio can be obtained. With the increasement of selenium in the film, the optical bandgap of $Sb_2(S,Se)_3$ films decreases from 1.69 to 1.48 eV, and the valence band maximum gradually shifts upward while the conduction band minimum remains nearly unchanged. Eventually, the planar device yielded a PCE of 5.8% (Tab. 1).

Further investigations on the interfacial engineering can be conducted by introducing indium-doped CdS (In:CdS) interlayer between $Sb_2(S,Se)_3$ and TiO_2 electron transporting layer (ETL)[17]. Compared with CdS film, the In:CdS interlayer allows more efficient light harvesting due to the increased band gap and alleviates thermodynamic loss in the photovoltaic energy conversion. Thus, the champion $Sb_{1.99}S_{2.11}Se_{0.91}$ planar-heterojunction device based on In:CdS interlayer delivered a PCE of 6.63%. However, there is a dissolution limit for selenium by using this thiol-amine mixture solvent and it is thus difficult to further

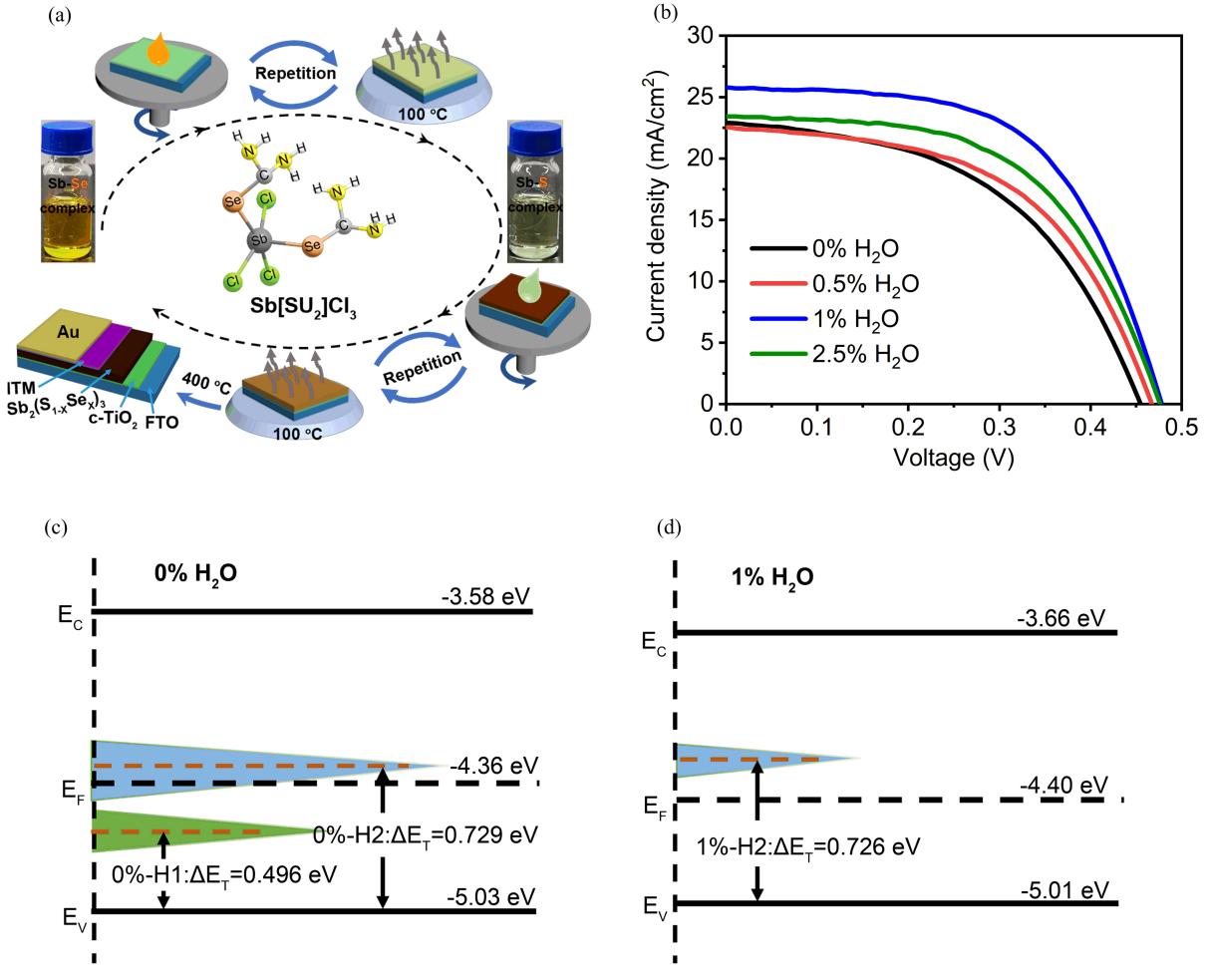

Fig. 6 (a) Schematic illustration of the fabrication process of $Sb_2(S,Se)_3$ solar cells. (b) J-V curves of $Sb_2(S,Se)_3$ devices fabricated without and with various amount of water additive in precursor solution. Energy states and defect level of the $Sb_2(S,Se)_3$ films with (c) 0% H_2O and (d) 1% H_2O additive in the precursor solution. Reproduced with permission from Ref.[18]. Copyright 2020, Wiley-VCH.

decrease the bandgap of $Sb_2(S,Se)_3$ film by simply adding more selenium.

To obtain narrower-bandgap $Sb_2(S,Se)_3$ thin film, a multi-step spin-coating process was developed to synthesize $Sb_2(S,Se)_3$ alloy thin films (Fig. 6(a))[18]. The precursor solution of Sb-Se complex was first spin-coated on the TiO_2 substrate, followed by heating on a hotplate to solidify the film. This process was repeated twice to increase the thickness of Sb-Se precursor film. Subsequently, two-cycle spin-coating of Sb-S complex solution on the Sb-Se precursor film was conducted in a similar manner. Upon annealing, S and Se atoms are interdiffused between Sb-Se and Sb-S precursor film to form crystalline $Sb_2(S,Se)_3$ alloy thin film. Additionally, it is found that a tiny amount of water (1% volume) in the solution enables an essential increasement in grain size and optimum bandgap (1.35 eV). The improved film quality leads to an efficiency of 7.42% for alloy $Sb_2(S,Se)_3$-based solar cells with planar heterojunction device configuration of FTO/TiO_2/$Sb_2(S,Se)_3$/spiro-OMeTAD/Au (Fig. 6(b)). According to the deep-level transient spectroscopy (DLTS) characterization (Fig. 6 (c), (d)), the control device without water exhibits two kinds of hole (H1 and H2) trap defects and the device with 1% H_2O incorporation shows only lower-density H2 defect, while the H1 defect was completely suppressed. However, the specific defect type was not assigned in this investigation.

Compared with the one-step spin-coating process, the grain size and compactness of $Sb_2(S,Se)_3$ films prepared by multi-step spin-coating method is enhanced and the bandgap is also optimized, resulting in a PCE increasement. Nonetheless, $Sb_2(S,Se)_3$ films prepared by both spin-coating methods displays a considerable amount of voids and pinholes, which usually cause severe carrier recombination and hinder device performance improvement. It is well known that compact and uniform film is essential for efficient solar cells. Further optimization on $Sb_2(S,Se)_3$ film quality is thus urgently needed.

2.3 Hydrothermal deposition method

Hydrothermal synthesis is conducted in a high-

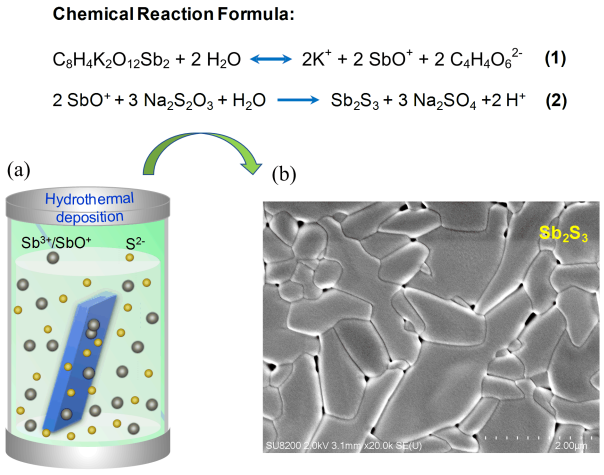

Fig. 7 (a) Chemical reaction process and schematic diagram of hydrothermal deposition and (b) surface morphology image of Sb_2S_3 film.

temperature aqueous solution at a high vapor pressure, which generates supercritical solvent for improving the solubility of the precursor materials. This method has been frequently applied in the synthesis of inorganic nanomaterials in the past decades. Recently, hydrothermal technique was demonstrated as an effective method for the deposition of Sb_2S_3 and $Sb_2(S,Se)_3$ films. In the synthesis of Sb_2S_3 thin film, potassium antimony tartrate ($C_8H_4K_2O_{12}Sb_2 \cdot xH_2O$) and sodium thiosulfate ($Na_2S_2O_3$) serve as the Sb and S sources (Fig. 7(a)), which generates flat and compact Sb_2S_3 films (Fig. 7(b)). The post-selenization can transfer the surface Sb_2S_3 to $Sb_2(S,Se)_3$[19]. With the optimization of selenization temperature, an encouraging efficiency of 6.14% was acquired[20].

Since only superficial Sb_2S_3 is translated into $Sb_2(S,Se)_3$, the average band gap is 1.63 eV. To improve the PCE of $Sb_2(S,Se)_3$ solar cells, our group demonstrated a pathway to acquiring high-quality alloy $Sb_2(S,Se)_3$ film with compact morphology and appropriate bandgap via hydrothermal process[21]. The critical process in this synthesis is the introduction of selenourea in the reaciton system as Se precursor. This deposition generates $Sb_2(S,Se)_3$ films with the band gap of 1.45 eV. The film also shows homogenous lateral distribution of S and Se (Fig. 8(a), (b)). An interesting finding in this study is that the increase of Se/S ratio in the $Sb_2(S,Se)_3$ film facilitated tilted $[Sb_4S(e)_6]_n$ ribbons on the substrate, which enables efficient carrier transport (Fig. 8(c), (d)). Additionally, appropriate Se component led to a decreased number and density of deep-level defects. Eventually, the $Sb_2(S,Se)_3$ solar cell delivered a landmark efficiency of 10.0% (Fig. 8(e)). Furthermore, in order to control the nucleation and deposition process for obtaining high-quality $Sb_2(S,Se)_3$ films, a strong coordination additive of ethylenediaminetetraacetic acid (EDTA) achieved a PCE of 10.5% for $Sb_2(S,Se)_3$ solar cell[22].

This kind of $Sb_2(S,Se)_3$ film can also form heterojunction with perovskite quantum dots (QDs) for solar cell applications, where QDs such as $CH_3NH_3PbBr_3$ and $CsPbBr_3$ serve as highly efficient and air-stable HTMs (Fig. 9(a))[23]. The device based on $CsPbBr_3$ QDs/$Sb_2(S,Se)_3$ heterojunction generates PCE of 7.82% (Fig. 9(b)). Remarkably, the device exhibits no decline in PCE after being stored in ambient air for over 100 d (Fig. 9(c)).

3 Prospects of $Sb_2(S,Se)_3$ solar cells

At the present stage, improving the efficiency is one of the most important tasks in the $Sb_2(S,Se)_3$ solar cell development. Here, we suggest the following aspects to further improve the device performance.

3.1 Seeking suitable film preparation methods and device configuration

High-quality absorber film is crucial for the delivery of high-efficiency solar cells. There are several basic requirements for high-quality film: high purity, high crystallinity, large grain size, compact and smooth morphology. These characteristics are able to minimize grain boundary, reduce undesirable recombination losses and enhance the charge carrier transport ability across the films. In general, the aforementioned solution-processed $Sb_2(S,Se)_3$ films exhibit low crystallinity and contain some impurities such as carbon residues. In particular, even the hydrothermal deposition delivered 10.5% PCE, the crystallinity and the grain size are not large. Optimizing the deposition process and post annealing seem promising to further improve the film quality. Vacuum method, in contrast, is able to generate high-purity, high-crystallinity and large-grain $Sb_2(S,Se)_3$ films[31-33], which is promising for the fabrication of high-efficiency solar cells. The initial application of vacuum deposition derived $Sb_2(S,Se)_3$ generated an encouraging efficiency of 7.27%[34]. To insightfully examine the optical, electrical and defect properties of the as-synthesized film, establishing the correlation between fabrication approach and properties of the as-synthesized film is required for further development.

Different from 3D crystal structures, controlling over the microstructure of $Sb_2(S,Se)_3$ film is one of the key factors in achieving high efficiency solar cells due to the anisotropic physical properties[5,6]. One of the critical parameters for controlling the orientation is the substrate, the initial coordination between absorber materials and the substrate plays a critical role in determining the crystal growth[35-36]. For instance, it has been observed that Mo-coated substrate facilitates [hk1]-orientated Sb_2Se_3 film[37-39]. This growth habit is also found to associate with the S/Se elements in the hydrothermal synthesis[21]. Probably, deposition of $Sb_2(S,Se)_3$ film on Mo-coated substrate via hydrothermal process may be a feasible way.

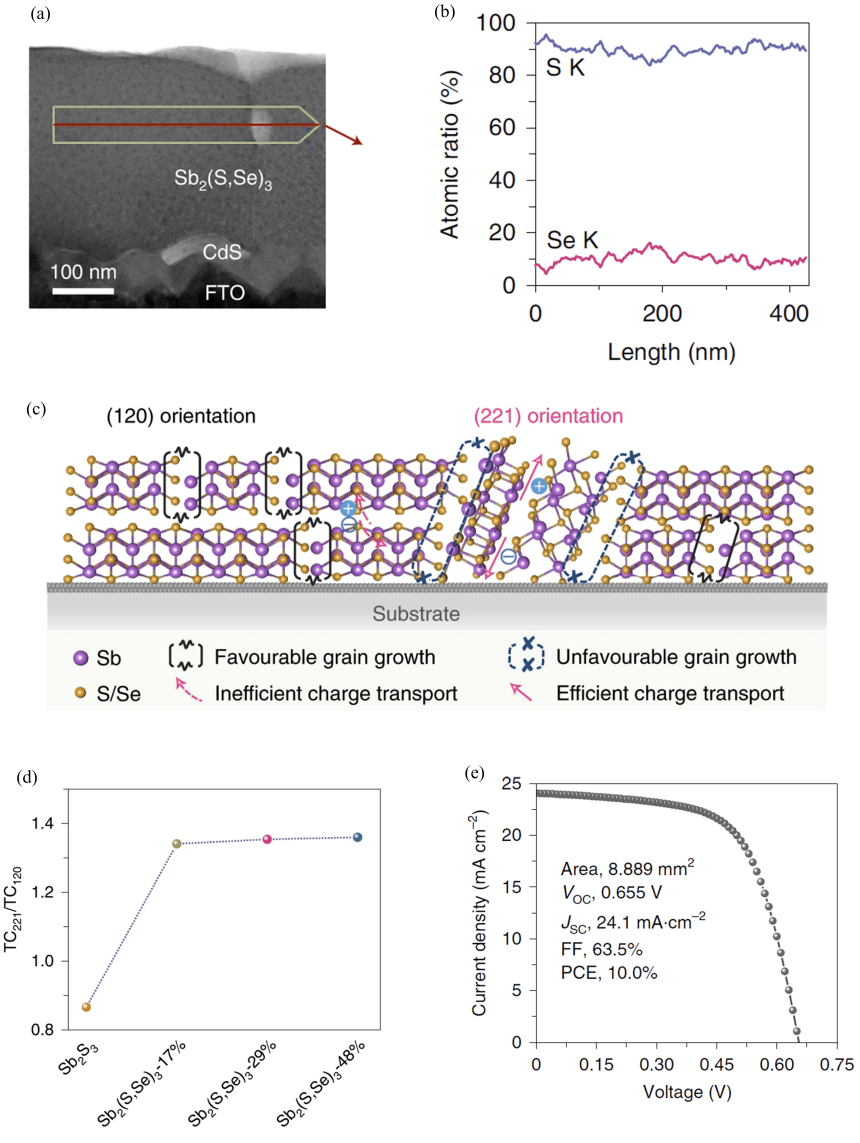

Fig. 8 (a) Cross-sectional SEM image of an FTO/CdS/$Sb_2(S,Se)_3$ film. (b) EDS line scan profile along the marked area of the $Sb_2(S,Se)_3$ film. (c) Atomic structure illustration of the oriented $[Sb_4S(e)_6]_n$ ribbons and the impact on grain growth. (d) Texture coefficient ratio between the (221) and (120) crystal planes of the various Sb_2S_3 and $Sb_2(S,Se)_3$ films. (e) The certified J-V curve and the corresponding photovoltaic parameters of the best $Sb_2(S,Se)_3$ device. Reproduced with permission from Ref.[21]. Copyright 2020, Nature Publishing Group.

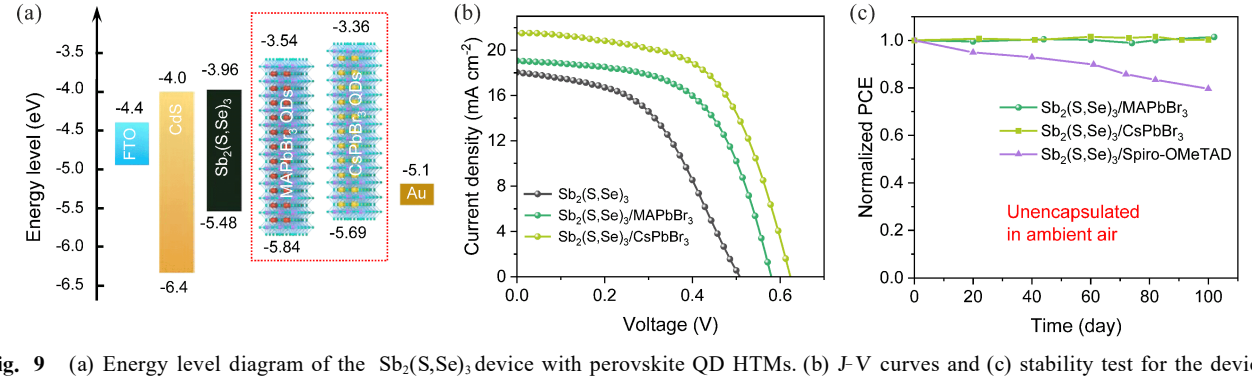

Fig. 9 (a) Energy level diagram of the $Sb_2(S,Se)_3$ device with perovskite QD HTMs. (b) J-V curves and (c) stability test for the devices with different HEMs. Reproduced with permission from Ref.[23]. Copyright 2019, Cell Press.

3.2 Effective defect passivation

Defects have a crucial influence on device performance by causing a degradation of optical and electrical properties. It is confirmed that high-concentration defects exist in $Sb_2(S,Se)_3$ film and free carrier concentration of undoped $Sb_2(S,Se)_3$ ($\sim 10^{13}$ cm^{-3}) is much lower than the optimal value of 10^{16} cm^{-3} for well-established solar cells[40]. Besides, the longest carrier lifetime in $Sb_2(S,Se)_3$ ($\sim$9 ns) is far inferior to that of the well-developed CdTe ($\sim$3.6 μs), CIGS (250 ns), and lead halogen perovskite ($>$1 μs). These factors lead to severe open-circuit voltage deficit (defined as E_g/e-V_{oc}) of the $Sb_2(S,Se)_3$ solar cells, even exceeding half of the E_g value ($>$0.7 V). It is also much worse than that of CIGS (0.416 V), CdTe (0.593 V), and CZTS (0.617 V) solar cells[7]. To address these issues, seeking effective doping elements like P, Cl, Pb, Sn and means[41], surface and interface passivation is believed to be an effective way to realize the defects passivation, grain-size enhancement, conductivity increase and so on.

3.3 Exploitation of appropriate charge transport layer

To date, CdS ETL has been most frequently used in reported high-efficiency $Sb_2(S,Se)_3$ solar cells above 7% (Tab. 1)[3,21,34,37]. Nonetheless, CdS is toxic, and absorbs a significant portion of the incident light due to its small bandgap ($\sim$2.4 eV). It also leads to an unsatisfactory device stability because of the possible Cd diffusion in high-temperature processing[5]. On the premise of achieving outstanding device performance, a non-toxic and wide-bandgap ETL alternative seems to be the best choice. In addition, regulating the crystal and morphology of ETL could also affect the crystal orientation of the $Sb_2(S,Se)_3$ film.

In terms of HTMs, many inorganic and organic materials such as PbS[42], CuSCN[43], V_2O_5[44], PEDOT[11], spiro-OMeTAD[21], P3HT[45] and PCDTBT[46] have been selected to improve the device performance. In contrast to organic HTMs, the function of inorganic HTMs is less studied. Nonetheless, efficient organic HTMs are in general expensive, and the hygroscopic dopants in organic HTMs would significantly affect the long-term stability of the devices. Therefore, low-cost, stable, and S-containing HTM (i.e., dopant-free organic polymers or small molecules; transition metal sulfide, MoS, WS_2, MnS) shall be alternatives to enhance the contact quality and charge transfer efficiency and device performance.

Overall, $Sb_2(S,Se)_3$ is a promising next-generation solar cell material with superior photovoltaic properties and high stability. Although the PCE of $Sb_2(S,Se)_3$ solar cells lags behind other well-established thin-film solar cells, the gradually increased efficiency and in-depth understanding of the material's properties highlight the great potential as an emerging light harvesting material.

Acknowledgments

This work was supported by the National Key Research and Development Program ofChina (2019YFA0405600), the National Natural Science Foundation of China (U19A2092, 22005293).

Conflict of interest

The authors declare no conflict of interest.

Author information

JIANG Chenhui is a Ph.D. student under the supervision of Prof. Chen Tao at University of Science and Technology of China (USTC). He received his bachelor's degree in Material Science and Engineering from China University of Mining and Technology (CUMT) in 2016. His research mainly focuses on the preparation of antimony sulfide-selenide ($Sb_2(S,Se)_3$) thin films and hole-transporting materials for $Sb_2(S,Se)_3$ solar cells.

TANG Rongfeng is a post-doctor under the supervision of Prof. Chen Tao at University of Science and Technology of China. She received her B.S. and M.S. degree from Liaocheng University in 2013 and 2016, respectively, and Ph. D. degree from University of Science and Technology of China in 2019. Her research focuses on synthesis of nanomaterials and preparation of solar photovoltaic devices. She has published research papers in *Nature Energy*, *Journal of Materials Chemistry A*, *ACS Applied Materials & Interfaces*, etc.

ZHU Changfei (corresponding author) is Full Professor at the department of materials science and engineering, University of Science and Technology of China. He received his B. S. and Ph.D. degrees both from University of Science and Technology of China in 1984 and 1990, respectively. Afterwards, he was working in department of materials science and engineering, University of Science and Technology of China. His research interests include fundamental study and application of transitional metal oxide, wide band gap semiconductor and new concept solar cells.

CHEN Tao (corresponding author) is Full Professor at the department of materials science and engineering, University of Science and Technology of China. He received his Ph.D. degree in Chemistry from Nanyang Technological University (Singapore) in 2010. From 2011 to 2015 he joined the Department of Physics, the Chinese University of Hong Kong, working as a research assistant professor. His

research interests include materials science, fabrication and engineering of antimony sulfide-selenide ($Sb_2(S,Se)_3$) solar cells. He has published more than 100 papers in peer reviewed journals, including *Nature Energy*, *Nature Communications*, *Science Bulletin*, etc.

References

[1] Kondrotas R, Chen C, Tang J. Sb_2S_3 solar cells. Joule, 2018, 2(5): 857-878.

[2] Lei H W, Chen J J, Tan Z J, et al. Review of recent progress in antimony chalcogenide-based solar cells: Materials and devices. Solar RRL, 2019, 3(6): 1900026.

[3] Wen X, Chen C, Lu S, et al. Vapor transport deposition of antimony selenide thin film solar cells with 7.6% efficiency. Nat. Commun., 2018, 9(1): 2179.

[4] Jiang C, Tang R, Wang X, et al. Alkali metals doping for high-performance planar heterojunction Sb_2S_3 solar cells. Solar RRL, 2019, 3(1): 1800272-1800280.

[5] Wang L, Li D B, Li K, et al. Stable 6%-efficient Sb_2Se_3 solar cells with a ZnO buffer layer. Nat. Energy, 2017, 2(4): 17046.

[6] Li K, Chen C, Lu S, et al. Orientation engineering in low-dimensional crystal-structural materials via seed screening. Adv. Mater., 2019, 31: 1903914.

[7] Chen C, Tang J. Open-circuit voltage loss of antimony chalcogenide solar cells: Status, origin, and possible solutions. ACS Energy Lett., 2020, 5(7): 2294-2304.

[8] Huang M, Xu P, Han D, et al. Complicated and unconventional defect properties of the quasi-one-dimensional photovoltaic semiconductor Sb_2Se_3. ACS Appl. Mater. Interfaces, 2019, 11(17): 15564-15572.

[9] Zhou Y, Wang L, Chen S, et al. Thin-film Sb_2Se_3 photovoltaics with oriented one-dimensional ribbons and benign grain boundaries. Nat. Photonics, 2015, 9(6): 409-415.

[10] Deng H, Yuan S, Yang X, et al. High-throughput method to deposit continuous composition spread $Sb_2(Se_xS_{1-x})_3$ thin film for photovoltaic application. Prog. Photovolt. Res. Appl., 2018, 26(4): 281-290.

[11] Choi Y C, Lee D U, Noh J H, et al. Highly improved Sb_2S_3 sensitized-inorganic-organic heterojunction solar cells and quantification of traps by deep-level transient spectroscopy. Adv. Funct. Mater., 2014, 24(23): 3587-3592.

[12] Calixto-Rodriguez M, García H M, Nair M T S, et al. Antimony chalcogenide/lead selenide thin film solar cell with 2.5% conversion efficiency prepared by chemical deposition. ECS J. Solid State Sci. Technol., 2013, 2(4): Q69-Q73.

[13] Choi Y C, Lee Y H, Im S H, et al. Efficient inorganic-organic heterojunction solar cells employing $Sb_2(S_x/Se_{1-x})_3$ graded-composition sensitizers. Adv. Energy Mater., 2014, 4(7): 1301680.

[14] Zhang Y, Li J, Jiang G, et al. Selenium-graded $Sb_2(S_{1-x}Se_x)_3$ for planar heterojunction solar cell delivering a certified power conversion efficiency of 5.71%. Solar RRL, 2017, 1(5): 1700017-1700024.

[15] Wang W, Chen G, Wang Z, et al. Full-inorganic $Sb_2(S,Se)_3$ solar cells using carbon as both hole selection material and electrode. Electrochim. Acta, 2018, 290: 457-464.

[16] Wu C, Zhang L, Ding H, et al. Direct solution deposition of device quality $Sb_2S_{3-x}Se_x$ films for high efficiency solar cells. Sol. Energ. Mat. Sol. C., 2018, 183: 52-58.

[17] Wu C, Jiang C, Wang X, et al. Interfacial engineering by indium-doped CdS for high efficiency solution processed $Sb_2(S_{1-x}Se_x)_3$ solar cells. ACS Appl. Mater. Interfaces, 2019, 11(3): 3207-3213.

[18] Wu C, Lian W, Zhang L, et al. Water additive enhanced solution processing of alloy $Sb_2(S_{1-x}Se_x)_3$-based solar cells. Solar RRL, 2020, 4(5): 1900582-1900590.

[19] Wang W, Wang X, Chen G, et al. Promising $Sb_2(S,Se)_3$ solar cells with high open voltage by application of a TiO_2/CdS double buffer layer. Solar RRL, 2018, 2(11): 1800208-1800216.

[20] Wang W, Wang X, Chen G, et al. Over 6% certified $Sb_2(S,Se)_3$ solar cells fabricated via in situ hydrothermal growth and postselenization. Adv. Electron. Mater., 2019, 5(2): 1800683.

[21] Tang R, Wang X, Lian W, et al. Hydrothermal deposition of antimony selenosulfide thin films enables solar cells with 10% efficiency. Nat. Energy, 2020, 5(8): 587-595.

[22] Wang X M, Tang R F, Jiang C H, et al. Manipulating the electrical properties of $Sb_2(S,Se)_3$ film for high-efficiency solar cell. Adv. Energy Mater., 2020, 10(40): 2002341.

[23] Jiang C H, Yao J S, Huang P, et al. Perovskite quantum dots exhibiting strong hole extraction capability for efficient inorganic thin film solar cells. Cell Rep. Phys. Sci., 2020, 1(1): 100001.

[24] Mughal M A, Engelken R, Sharma R. Progress in indium (III) sulfide (In_2S_3) buffer layer deposition techniques for CIS, CIGS, and CdTe-based thin film solar cells. Solar Energy, 2015, 120: 131-146.

[25] Li J M, Huang L, Hou J, et al. Effects of substrate orientation and solution movement in chemical bath deposition on Zn(O,S) buffer layer and $Cu(In,Ga)Se_2$ thin film solar cells. Nano Energy, 2019, 58: 427-436.

[26] Choi Y C, Mandal T N, Yang W S, et al. Sb_2Se_3-sensitized inorganic-organic heterojunction solar cells fabricated using a single-source precursor. Angew. Chem. Int. Ed., 2014, 53(5): 1329-1333.

[27] Chang J A, Rhee J H, Im S H, et al. High-performance nanostructured inorganic-organic heterojunction solar cells. Nano Lett., 2010, 10(7): 2609-2612.

[28] Kim D H, Lee S J, Park M S, et al. Highly reproducible planar Sb_2S_3-sensitized solar cells based on atomic layer deposition. Nanoscale, 2014, 6(23): 14549-14554.

[29] Yang B, Xue D J, Leng M, et al. Hydrazine solution processed Sb_2S_3, Sb_2Se_3 and $Sb_2(S_{1-x}Se_x)_3$ film: molecular precursor identification, film fabrication and band gap tuning. Sci. Rep., 2015, 5: 10978.

[30] McCarthy C L, Webber D H, Schueller E C, et al. Solution-phase conversion of bulk metal oxides to metal chalcogenides using a simple thiol-amine solvent mixture. Angew. Chem. Int. Ed., 2015, 54(29): 8378-8381.

[31] Lu S, Zhao Y, Wen X, et al. $Sb_2(Se_{1-x}S_x)_3$ thin-film solar cells fabricated by single-source vapor transport deposition. Solar RRL, 2019, 3(4): 1800280-1800287.

[32] Ishaq M, Deng H, Yuan S, et al. Efficient double buffer layer $Sb_2(Se_xS_{1-x})_3$ thin film solar cell via single source evaporation. Solar RRL, 2018, 2(10): 1800144.

[33] Chen C, Yin Y W, Lian W T, et al. Pulsed laser deposition of antimony selenosulfide thin film for efficient solar cells. Appl. Phys. Lett., 2020, 116(13): 133901.

[34] Li K, Lu Y, Ke X, et al. Over 7% efficiency of $Sb_2(S,Se)_3$ solar cells via V-shaped bandgap engineering. Solar RRL, 2020, 4(9): 2000220-2000227.

[35] Jin X, Fang Y, Salim T, et al. In situ growth of [hk1]-oriented Sb_2S_3 for solution-processed planar heterojunction solar cell with 6.4% efficiency. Adv. Funct. Mater., 2020, 30(35): 2002887.
[36] Deng H, Zeng Y, Ishaq M, et al. Quasiepitaxy strategy for efficient full-inorganic Sb_2S_3 solar cells. Adv. Funct. Mater., 2019, 29(31): 1901720-1901730.
[37] Li Z, Liang X, Li G, et al. 9.2%-efficient core-shell structured antimony selenide nanorod array solar cells. Nat. Commun., 2019, 10(1): 125.
[38] Liang G X, Luo Y D, Chen S, et al. Sputtered and selenized Sb_2Se_3 thin-film solar cells with open-circuit voltage exceeding 500 mV. Nano Energy, 2020,73: 104806.
[39] Guo C, Liang X, Liu T, et al. 1D/3D alloying induced phase transition in light absorbers for highly efficient Sb_2Se_3 solar cells. Solar RRL, 2020, 4(4): 2000054-2000062.
[40] Chen C, Bobela D C, Yang Y, et al. Characterization of basic physical properties of Sb_2Se_3 and its relevance for photovoltaics. Front. Optoelectron., 2017, 10(1): 18-30.
[41] Cai Z H, Chen S Y. Extrinsic dopants in quasi-one-dimensional photovoltaic semiconductor Sb_2S_3: A first-principles study. J. Appl. Phys., 2020, 127(18): 183101.
[42] Chen C, Wang L, Gao L, et al. 6.5% certified efficiency Sb_2Se_3 solar cells using PbS colloidal quantum dot film as hole-transporting layer. ACS Energy Lett., 2017, 2(9): 2125-2132.
[43] Li K H, Wang S Y, Chen C, et al. 7.5% n-i-p Sb_2Se_3 solar cells with CuSCN as a hole-transport layer. J. Mater. Chem. A, 2019, 7(16): 9665-9672.
[44] Zhang L J, Jiang C H, Wu C Y, et al. V_2O_5 as hole transporting material for efficient all inorganic Sb_2S_3 solar cells. ACS Appl. Mater. Interfaces, 2018, 10(32): 27098-27105.
[45] Fukumoto T, Moehl T, Niwa Y, et al. Effect of interfacial engineering in solid-state nanostructured Sb_2S_3 heterojunction solar cells. Adv. Energy Mater., 2013, 3(1): 29-33.
[46] Choi Y C, Seok S I. Efficient Sb_2S_3-sensitized solar cells via single-step deposition of Sb_2S_3 using S/Sb-ratio-controlled $SbCl_3$-thiourea complex solution. Adv. Funct. Mater., 2015, 25(19): 2892-2898.

溶液法制备硒硫化锑太阳能电池最新研究进展

江晨辉,唐荣风,朱长飞*,陈 涛*
中国科学技术大学材料科学与工程系,中国科学院能量转换材料重点实验室,合肥微尺度物质科学国家研究中心,安徽合肥 230026

摘要: 硒硫化锑[$Sb_2(S,Se)_3$]具有良好的光电性能,例如强的吸收系数、可在 1.1～1.7 eV 范围内调节的光学带隙.在实际应用方面,该化合物材料环境友好、所含元素地壳储量丰富、对水和氧气性质稳定.最近的研究成果已将 $Sb_2(S,Se)_3$ 太阳能电池的光电转换效率突破 10%,表明 $Sb_2(S,Se)_3$ 具有重要的研究价值和潜在的应用前景.本文首先介绍 $Sb_2(S,Se)_3$ 的基本性质,包括化学结构、晶体结构以及光电性质等.随后,重点介绍近三年来溶液法制备 $Sb_2(S,Se)_3$ 太阳能电池的重要进展.最后,我们提出 $Sb_2(S,Se)_3$ 太阳能电池效率提升的可能策略.

关键词: 太阳能电池;硒硫化锑;$Sb_2(S,Se)_3$;溶液法;水热沉积